UCRL-50667

D-2

UCRL-50667

released

Dr. Fletcher

A SIMPLE ANALYTICAL MODEL FOR THE DUST DEVIL

Samuel E. Logan

May 1969

Lawrence Radiation Laboratory
UNIVERSITY OF CALIFORNIA
LIVERMORE

TID-4500, UC-53
Meteorology

Lawrence Radiation Laboratory
UNIVERSITY OF CALIFORNIA
LIVERMORE

UCRL-50667

A SIMPLE ANALYTICAL MODEL FOR THE DUST DEVIL

Samuel E. Logan

Contents

Abstract 1

Introduction 1

The Model 5

The Ekman Inflow Layer 6

The Horizontal Velocity Fields in the Ekman Layer 6

The Vertical Velocity Field in the Ekman Layer 10

The Prandtl Layer 13

Discussion of Results 15

Specification of $\alpha(r)$ and $\eta(r)$ 15

Height of the Ekman Layer and Basic Boundary Layer Behavior of u, v, and w 16

Comparison with Kuo 17

Detailed Velocity Component Behavior and Comparison to Sinclair's Measurements 20

Conclusions 24

Acknowledgments 25

References 26

A SIMPLE ANALYTICAL MODEL FOR THE DUST DEVIL

Abstract

A simple analytical model was developed for prescribing the velocity fields in a dust devil, a small intense vortex phenomenon common in arid regions. The proposed model has a viscous "inner" region (boundary layer) composed of a Prandtl layer and an Ekman inflow layer and an inviscid "outer" region of cyclostrophic balance. Observations indicate that to a good approximation the outer flow is a Rankine combined vortex. Linearization of the equation of motion allows a solution for the radial and tangential velocities in the boundary layer and for the depth of the layer in terms of two parameters obtainable from observations: $\alpha(r)$, the inflow angle at the top of the Prandtl layer; and $\eta(r)$, a modified Ekman length determined by the outer flow. The vertical velocity field is then found by application of the continuity equation. The velocity fields are found to resemble a first-order solution by Kuo for convective atmospheric vortices, and compare reasonably with the measurements of Sinclair.

Introduction

Atmospheric thermals, vertical convective currents whose existence or initiation depends primarily on buoyancy, have for many years been of great scientific interest to meteorologists as well as of use to sailplane enthusiasts. A very interesting special case of atmospheric thermal is the dust devil, an intense vortex phenomenon found in arid regions where a thin thermal boundary layer with a highly super-adiabatic lapse rate develops due to solar surface heating.* Ives[2] reports that the lapse rate at the ground can exceed 2000 times the adiabatic value (see Fig. 1). Since an adiabatic lapse rate defines neutral static stability, such a thermal layer represents a large source of potential energy. This potential energy source and some initial vorticity are generally agreed to be the dominant factors in the formation of dust devils. Once started, the vortex is maintained by the inflow of fresh surface-heated environmental air (the fuel) toward the center (core) where buoyancy forces carry it aloft. The intense rotary motion is generated and sustained by the tendency of the air to conserve its angular momentum as it spirals toward the center. The rotation and the updraft result in a helical motion, usually made visible by entrained surface dust and debris that are carried aloft.

These dust columns vary in height from a few feet to nearly 2000 ft, but thermal currents above the vortex can persist to heights greater than 15,000 ft according to Sinclair's[3] sailplane measurements.

*Michelson[1] shows that a shear flow can provide a stabilizing influence to allow the formation of such a layer with a density inversion.

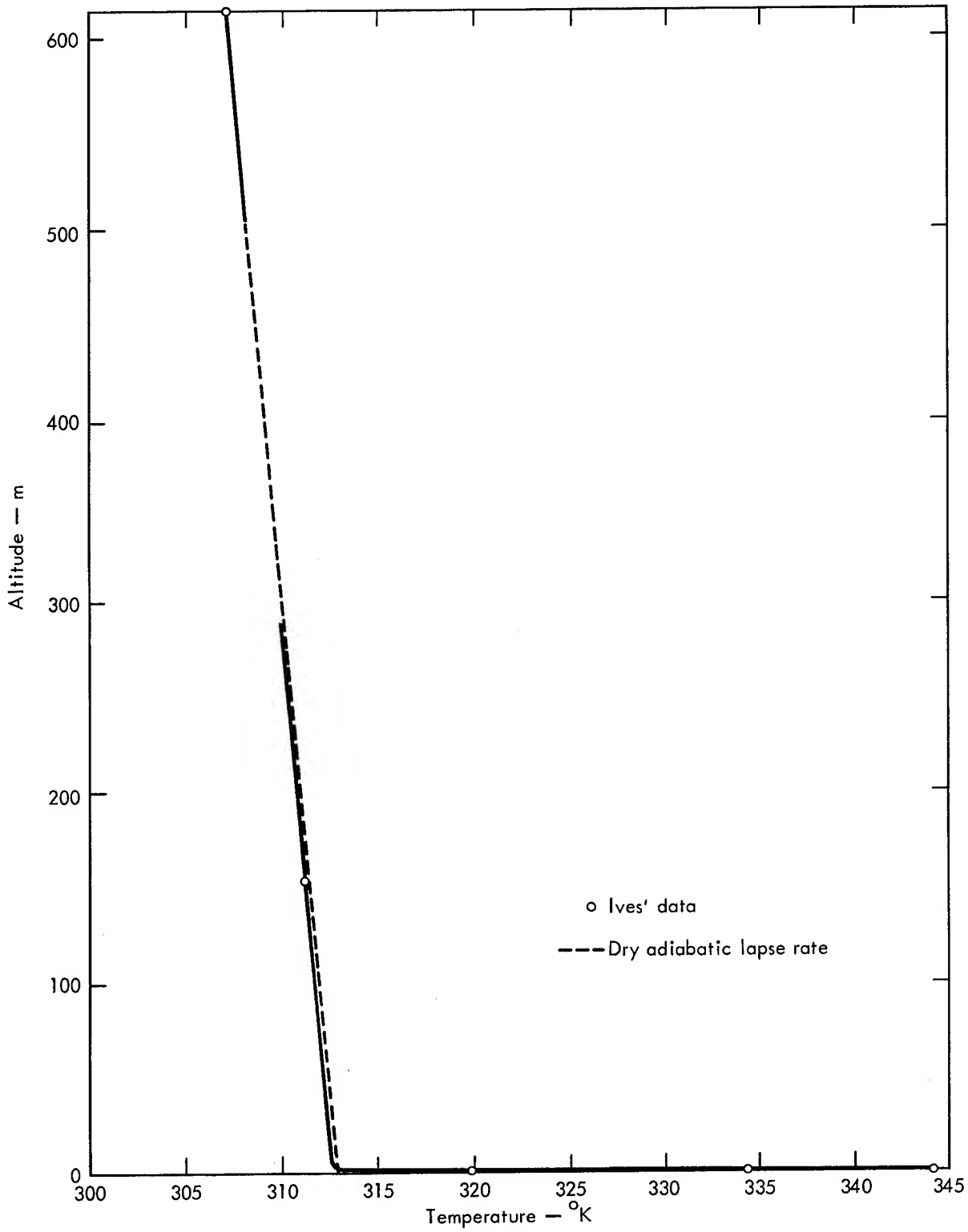

Fig. 1. Typical environmental temperature distribution favorable for the formation of dust devils. Ives (in "Behavior of the dust devil") shows that in a relatively thin surface layer of 2-3 m, the environmental lapse rate is strongly super-adiabatic. Although the exact temperature distribution in the region from z = 0 to z = 500 ft needs more data points, a plot of his data shows that above 500 ft, and probably some distance below it, the environmental lapse rate is essentially dry adiabatic.

Lifetimes vary from a few seconds to nearly 20 min, most lasting under 2 min.[4] Ives[2] observed an exceptional example during construction of a large railroad embankment near Sonora:

> In midmorning, a large dust devil suddenly appeared at the end of the embankment, and removed therefrom approximately one cubic yard of sand per hour for four hours. Erosion was halted, and the dust devil broken up, by parking a bulldozer at the end of the fill.

Dust devils depend directly on the availability of heated boundary-layer air and dissipate quickly if this fuel is removed.

The dust columns tend to meander across the desert floor at the prevailing wind speed. However, Sinclair has observed an apparent critical wind speed above which dust devil activity decreases, probably due to destruction of the heated boundary layer by increased vertical mixing and shearing of the vortices near the ground.[4]

The vertical velocities near the ground can be appreciable; Ives[2] made an early estimate of these by measuring the terminal velocities of small animals sometimes lifted by dust devils.*

However, the most detailed measurements of dust-devil velocity, pressure and temperature fields were made by Sinclair.[3] A typical set of his measurements, taken at altitudes of 7 and 31 ft are reproduced in Fig. 2. He measured tangential velocities approaching 15 m/sec, vertical velocities of 10 m/sec (at 7 ft), and maximum radial velocities of about 5 m/sec. Commonly, between the environment and the core there is a pressure drop in excess of 2 mb and a temperature increase of 4°C or more. As shown by Sinclair[3] in Fig. 3, the tangential flow resembles a Rankine combined vortex with a core of solid-body rotation and a free vortex outside. (Figures 2 and 3 are the same dust devil.)

The present analysis assumes an outer tangential flow from measurements by Sinclair,[3] Fig. 3, and determines the structure of the velocity fields in the inner flow region or boundary layer. All three velocity components are determined, the most interesting being the radial inflow, which supplies fresh fuel, and the vertical velocity, which carries it aloft. Also determined is the depth of the boundary layer, the height at which friction and radial inflow become negligibly small. Typical profiles are plotted and compared to a result by Kuo[5] and the measurements of Sinclair.[3]

---

*In his amusing acccount Ives notes that the kangaroo rat (terminal velocity ~25 mph) is "apparently unhurt after landing, although usually very angry," whereas a jackrabbit (terminal velocity ~35 mph) is "stunned and internally injured."

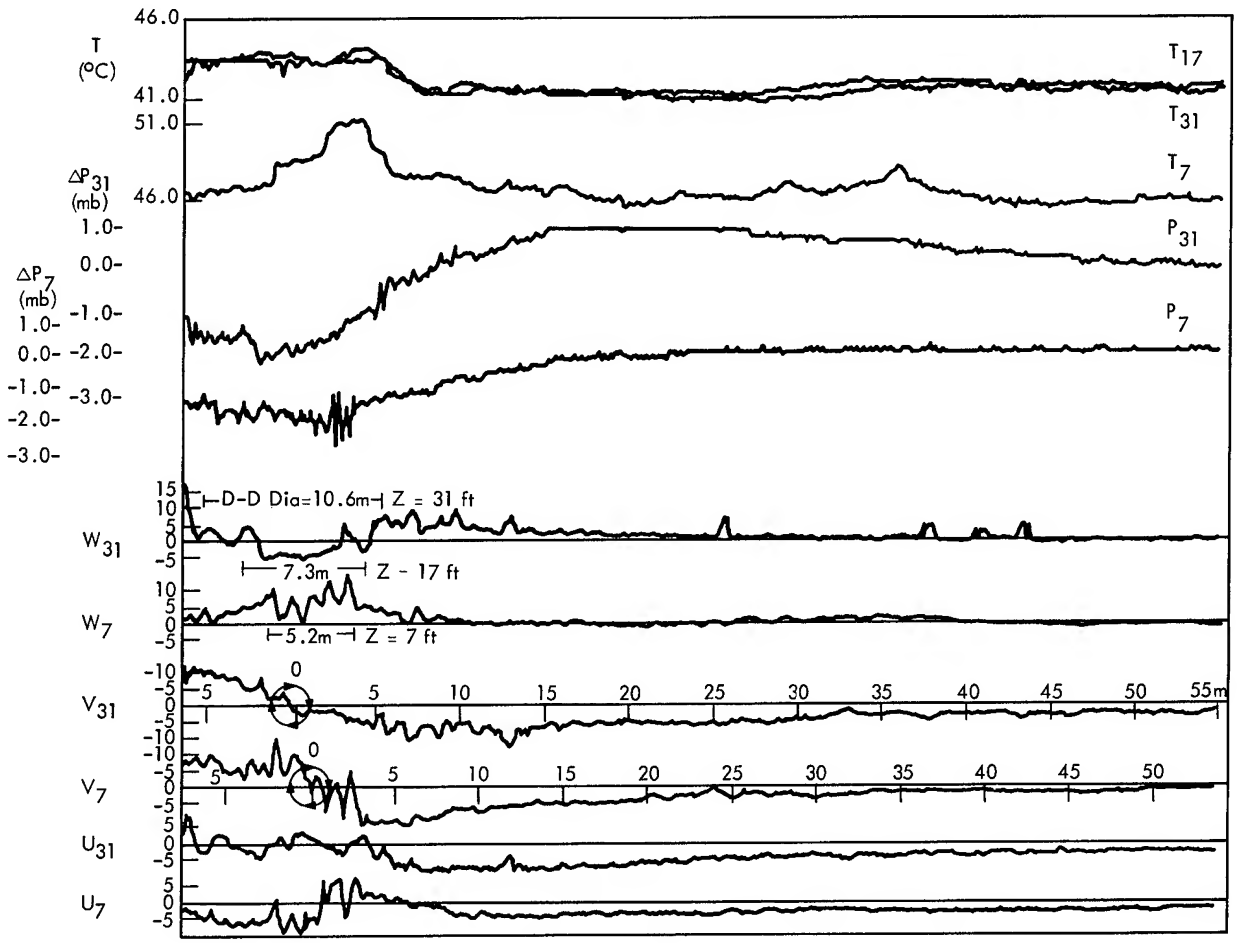

Fig. 2. Dust devil measurements (Fig. 4.2 from Sinclair's "A quantitative analysis of the dust devil") — temperature, pressure and wind velocity profiles across the base of dust devil moving to the left at 3 m sec^{-1}. The measurements were made in flat desert terrain on 13 August 1962, at 1300 MST near Tuscon, Arizona. The temperature profiles are at the top of the figure and represent temperatures (°C) along a horizontal line at the indicated heights of 7 ft, 17 ft (light line) and 31 ft. The lower temperature scale refers to the 7-ft profile and the upper scale to both 17-ft and 31-ft levels. Pressure profiles for the 7-ft and 31-ft levels are shown directly below the temperature data. The pressure scale is in millibars below the environmental pressure. The wind velocity is presented in terms of the three cylindrical components u, v, and w in $msec^{-1}$ for the 7-ft and 31-ft levels, and represents the velocity with respect to a coordinate system fixed to the ground. The negative signs on either side of zero for v7 and v31 merely indicate that the dust devil is rotating anti-cyclonically, which in cylindrical coordinates requires, by convention (right-hand system), a negative tangential component. The abscissa is the radial distance (meters) out from the dust devil center (defined as that point in which v changes direction and remains approximately 180 degrees from the wind before center passage). That is also the center of the cylindrical system at each level (i. e., r = 0). Due to the dust-devil slope, each level has a separate radial scale. The D-D Dia. refers to the width in meters of the dust column, at each level.

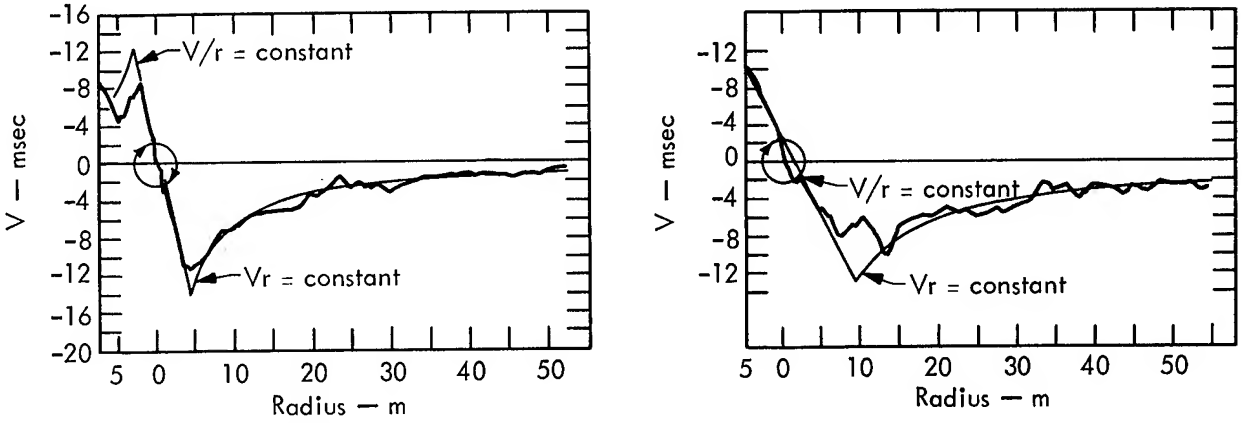

(a) Measurements at z = 7 ft

(b) Measurements at z = 31 ft

Fig. 3. Observed radial distribution of the mean tangential velocity at two levels in a dust devil, with superposed Rankine combined vortex profiles (Fig. 9.2 from Sinclair's "A quantitative analysis of the dust devil").

The Model

The axially symmetric velocity field is divided vertically into three main layers, as shown in Fig. 4. The lowest, or Prandtl, layer extends from the surface z = 0 to a

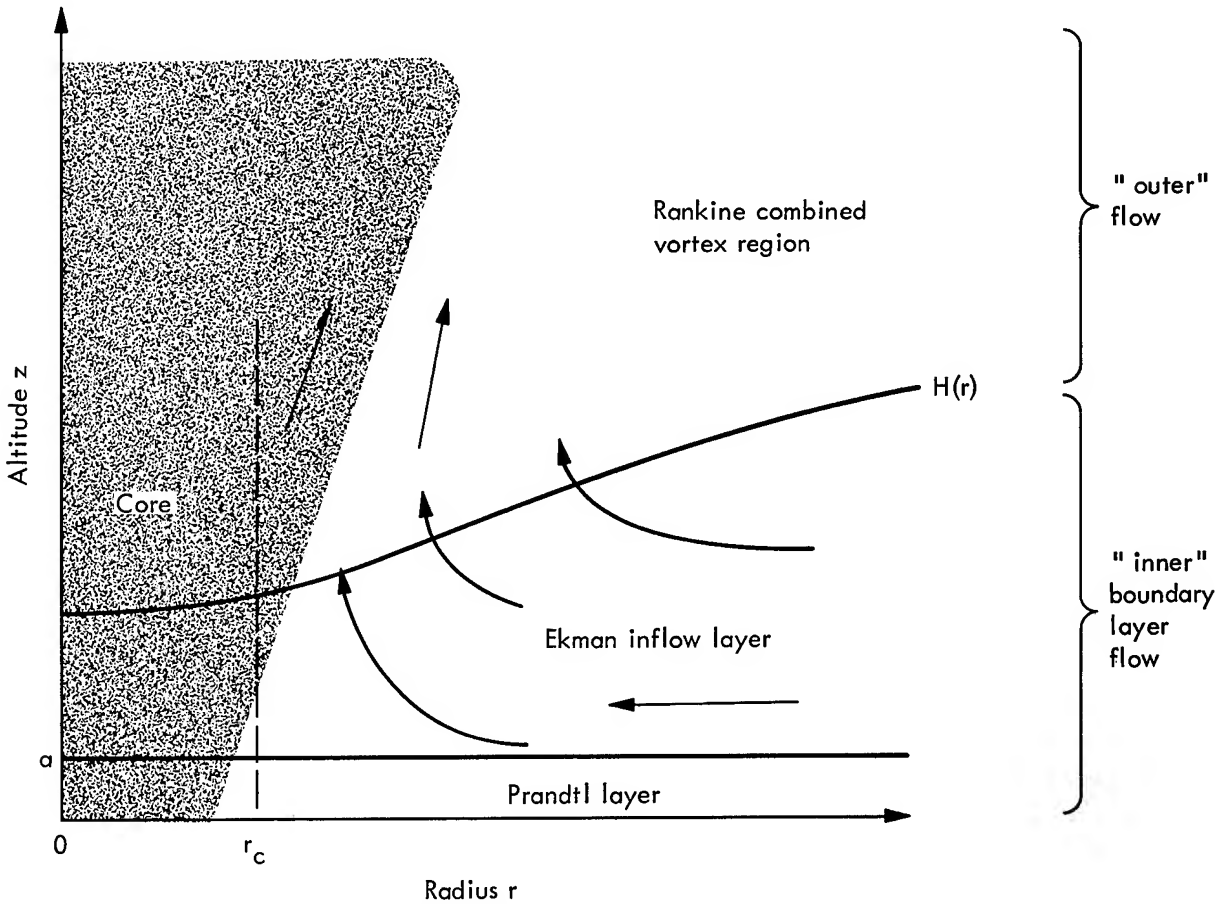

Fig. 4. Schematic diagram of the three main layers of the model.

level z = a which corresponds to the anemometer level for large-scale disturbances but is expected to be lower in the dust devil. In this layer the motion is controlled completely by the viscous drag on its upper and lower surfaces, and the velocity and vertical shear are assumed parallel. In the second or Ekman layer there is transition from the frictionally controlled radial inflow at z = a to a cyclostrophic balance at z = H(r), where H(r), the top of the Ekman layer, is a function of the radial distance from the vortex axis. In the upper layer z > H, viscous effects are assumed negligible, and the tangential motion everywhere satisfies the cyclostrophic-wind equation, Eq. (3). In accordance with observations (see Fig. 3) this tangential flow is assumed to be a Rankine combined vortex which has an interior ($r < r_c$) region of solid-body rotation and an exterior ($r > r_c$) region characterized by constant angular momentum. (Although Figs. 3a and 3b indicate that r_c, the "core radius," possibly increases with height, the simple model presented here assumes r_c to be constant throughout the three layers.) On the tangential flow there is superposed a vertical velocity resulting from the radial inflow below H and the requirement of mass continuity.

THE EKMAN INFLOW LAYER

The Horizontal Velocity Fields in the Ekman Layer

According to Ellsaesser[6] the vector equation of motion for steady, frictionally controlled, gradient flow* may be written

$$\nu \frac{\partial^2 \vec{V}}{\partial z^2} = 2\vec{\Omega}_z \times \vec{V} + \vec{\omega} \times \vec{V} - \text{grad}_h P, \tag{1}$$

where

$\vec{V}$ = horizontal wind vector = $v\hat{e}_\theta + u\hat{e}_r$
$\vec{\omega}$ = angular velocity = $v/r\ \hat{e}_z$
$2\vec{\Omega}_z$ = Coriolis parameter
ν = kinematic eddy viscosity
$\text{grad}_h P$ = horizontal gradient of pressure

For "large scale" atmospheric motions (e.g., geostrophic flow, hurricanes, etc.) the Coriolis term is dominant and existing solutions (Taylor[7] and Ellsaesser[6]) linearize about this term. However, for the much smaller-scale dust devil the centrifugal term is dominant and the Coriolis term is several orders of magnitude smaller.† Thus

---

*"Gradient flow" includes both Coriolis and centrigugal acceleration terms, whereas "geostrophic flow" includes only the Coriolis term and "cyclostrophic flow" includes only the centrifugal term.

†E.g., at 20° north, $2\Omega_z = 5 \times 10^{-5}$ sec^{-1}. For small r: v = 10 m/sec, r = 10 m, $\frac{V^2/r}{2\Omega_z V} = 2 \times 10^4$; for large r: V = 1 m/sec, r = 100 m, $\frac{V^2/r}{2\Omega_z V} = 2 \times 10^2$.

sufficient to describe the dust devil is the simpler, but nonlinear, equation for cyclostrophic flow:*

$$\nu \frac{\partial^2 \vec{V}}{\partial z^2} = \vec{\omega} \times \vec{V} - \text{grad}_h P. \tag{2}$$

To obtain an approximate solution to Eq. (2) we assume that friction becomes negligible at z = H and that $\text{grad}_h P$ and ν are constant in the layer $0 < z < H$. Then the cyclostrophic equation resulting from Eq. (2),

$$\text{grad}_h P = \vec{\omega}_c \times \vec{V}_c, \qquad \text{at } z = H \tag{3}$$

is valid throughout the Ekman layer, and Eq. (2) becomes

$$\nu \frac{\partial^2 \vec{V}}{\partial z^2} = \vec{\omega} \times \vec{V} - \vec{\omega}_c \times \vec{V}_c. \tag{4}$$

(At this point it should be emphasized that $\vec{V}$ and $\vec{\omega}$ are functions of r and z, and the outer-flow parameters $\vec{V}_c$ and $\vec{\omega}_c$ are functions of r. For clarity, functional dependence will not be indicated until the end.)

Equation (4) must be linearized to be solved. We make the convenient assumption that the tangential velocity, and thus $\vec{\omega}$, is constant in the Ekman layer. This is not a bad approximation, since Fig. 3 indicates less than a 10% change in the tangential velocity between z = 2 and 10 m. This linearizes the equation so that within the Ekman layer we now have

$$\nu \frac{\partial^2 \vec{V}}{\partial z^2} = \vec{\omega}_c \times (\vec{V} - \vec{V}_c). \tag{5}$$

Now Eq. (5) has the same form (but different constants) as the equation for the "Ekman spiral" for geostrophic flow as solved by Taylor.[7] Using Taylor's mathematical technique, we replace the velocity vectors $\vec{V}$ and $\vec{V}_c$ by complex numbers V and V_c (see Fig. 5). Then Eq. (5) may be written

$$\nu \frac{\partial^2 (V - V_c)}{\partial z^2} - i\, \omega_c (V - V_c) = 0,$$

---

*This is easily seen to reduce to the well-known cylindrical steady force-free Navier Stokes equation for r and θ.

It is quite important to note that, from Eq. (1), large-scale vortices such as hurricanes have a preferred direction of rotation because of the Coriolis term whose sign depends on the hemisphere. However, since this term is negligible in the dust devil, Eq. (2) implies that dust devils should have no such preferred direction, which is experimentally verified by Sinclair.[3]

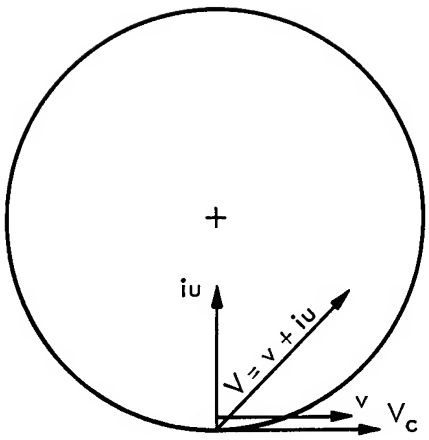

Fig. 5. Complex notation.

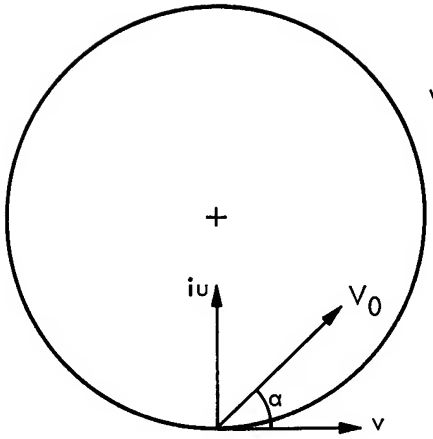

$V(a) = V_0 e^{i\alpha}$

$v = V_0 \cos\alpha$

$u = V_0 \sin\alpha$

Fig. 6. Inflow at top of Prandtl layer z = a.

since V_c is constant. This has the solution

$$V - V_c = ce^{-\eta(1+i)z} + de^{\eta(1+i)z},$$

where $\eta = (\omega_c/2\nu)^{1/2}$. We apply the following boundary conditions at z = a and H:

$$\begin{aligned} V(a) &= V_0 e^{i\alpha(r)} && \text{(see Fig. 6)} \\ &= \kappa\left(\mu \frac{\partial V}{\partial z}\right)_{z=a} && \text{(Prandtl's assumption)} \\ V - V_c &\to 0 \text{ as } z \to \infty && \text{(assumed valid at z = H)} \end{aligned} \tag{6}$$

where κ is simply a proportionality constant. These yield

$$d \equiv 0$$

$$c = \left(V_0 e^{i\alpha} - V_c\right) e^{\eta(1+i)a}.$$

We now have for the Ekman layer

$$V - V_c = \left(V_0 e^{i\alpha} - V_c\right) e^{-\eta(1+i)(z-a)}. \tag{7}$$

The corresponding value for the frictional stress τ is

$$\tau = \mu \frac{\partial V}{\partial z} = \sqrt{2}\mu\eta \left(V_0 e^{i\alpha} - V_c\right) e^{-\eta(1+i)(z-a)} e^{-3\pi i/4}.$$

Thus the stress forms an angle of $-\frac{3\pi}{4}$ with the cyclostrophic deviation $(V - V_c)$. At the level z = a we now have

$$V_0 e^{i\alpha} = \sqrt{2}\kappa\mu\eta \left(V_0 e^{i\alpha} - V_c\right) e^{-3\pi i/4},$$

which by separation into real and imaginary parts and simultaneous solution yields

$$V_0 = V_c (\cos\alpha - \sin\alpha) \tag{8}$$

and

$$\kappa = \frac{1}{2\mu\eta} (\cot\alpha - 1). \tag{9}$$

Combining Eqs. (7) and (8) and noting that

$$(\cos\alpha - \sin\alpha) e^{i\alpha} - 1 = -\sqrt{2} \sin\alpha e^{-i[(\pi/4)-\alpha]},$$

we obtain

$$v + iu = V_c \left\{1 - \sqrt{2} \sin\alpha e^{-\eta(z-a)-i[\eta(z-a)+(\pi/4)-\alpha]}\right\}, \tag{10}$$

which has the components

$$\begin{aligned} v(r, z) &= V_c(r)\left[1 - \sqrt{2} \sin\alpha \cos\left[\eta(z - a) + \frac{\pi}{4} - \alpha\right] e^{-\eta(z-a)}\right] \\ u(r, z) &= V_c(r)\sqrt{2} \sin\alpha \sin\left[\eta(z - a) + \frac{\pi}{4} - \alpha\right] e^{-\eta(z-a)} \end{aligned} \tag{11}$$

where $\alpha = \alpha(r)$ and $\eta = \eta(r)$.

The top of the Ekman layer ($z = H$) is defined as the height at which u first changes sign, i. e.,

$$\eta(H - a) + \frac{\pi}{4} - \alpha = \pi$$

or

$$H(r) = a + \frac{\frac{3\pi}{4} + \alpha(r)}{\eta(r)} . \tag{12}$$

By setting the z derivative of Eq. (11) to zero we find that the radial inflow, u, has a maximum at the level satisfying

$$\tan\left[\eta(z - a) + \frac{\pi}{4} - \alpha\right] = 1,$$

which implies

$$z_{u_{max}}(r) = a + \frac{\alpha(r)}{\eta(r)} . \tag{13}$$

Substitution of Eq. (13) into Eq. (11) yields the maximum radial velocity occurring at a given radius r:

$$u_{max}(r) = V_c(r) \sin \alpha(r) \, e^{-\alpha(r)} . \tag{14}$$

The Vertical Velocity Field in the Eckman Layer

Having found the radial-inflow velocity, u(r, z), everywhere in the Ekman layer ($a < z < H$), we use the axially symmetric continuity equation*

$$-\frac{1}{r}\frac{\partial(ru)}{\partial r} + \frac{\partial w}{\partial z} = 0 \tag{15}$$

to determine the vertical velocity, i. e.,

$$w(r, z) - w(r, a) = \int_a^z \frac{1}{r}\frac{\partial(ru)}{\partial r} \, dz \tag{16}$$

where w(r, a) is the vertical velocity at the top of the Prandtl layer, to be determined in the next section of this report.

As seen in the preceding analysis, the major parameters determining the radial inflow are $\alpha(r)$, the inflow angle at the top of the Prandtl layer, and $\eta(r)$, a modified Ekman length determined by $V_c(r)$, the cyclostrophic velocity at the top of the Ekman layer. In order to determine $\eta(r)$, we proceed to specify $V_c(r)$ in terms of V_m, the maximum tangential velocity in the Rankine combined vortex at the level z = H, as shown in Fig. 7. (Typically, V_m = 10-15 m/sec, and r_c = 5-10 m.)

Since $V_c(r)$ has different functional dependence in the two regions, we calculate w(z) separately for each.

Core Region, $0 < r < r_c$:

$$V_c = \frac{r}{r_c} V_m \quad \text{and} \quad \omega_c = \frac{V_c}{r} = \frac{V_m}{r_c} \equiv \text{constant.}$$

Therefore η = constant, and from Eq. (16) the vertical velocity is given by

$$w(r, z) - w(r, a) = \frac{V_m}{r_c} \left[2I_1(r, z) + rI_2(r, z) \right] , \tag{17}$$

*The negative sign is required on the r term because our u is positive when the flow is toward r = 0.

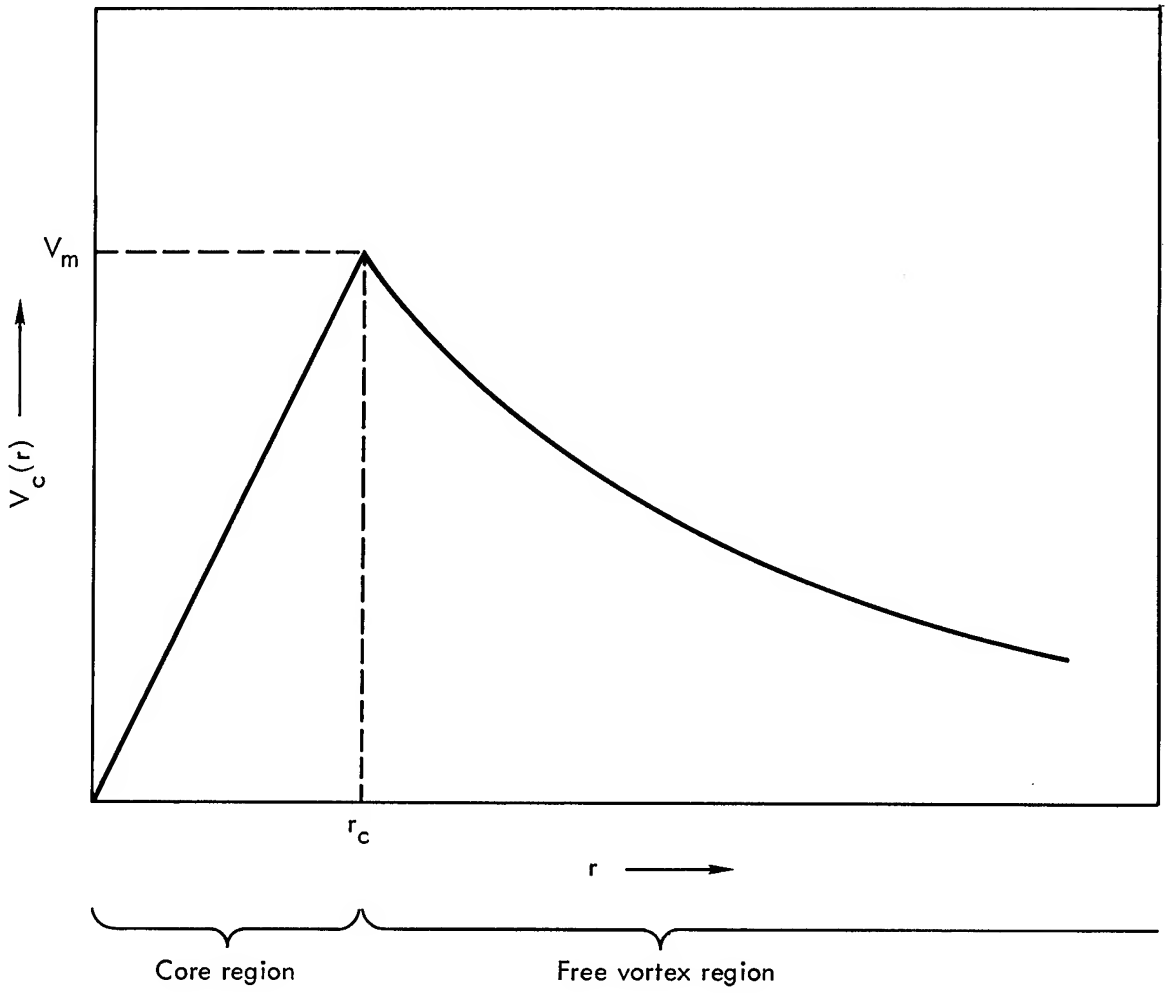

Fig. 7. Cyclostrophic velocity distribution, $V_c(r)$, above the Ekman layer.

in which

$$I_1(r, z) \equiv \sqrt{2} \sin \alpha(r) \int_a^z \sin \left[\eta(z - a) + \frac{\pi}{4} - \alpha(r)\right] e^{-\eta(z-a)} \, dz$$

and

$$I_2(r, z) \equiv \sqrt{2} \int_a^z e^{-\eta(z-a)} \frac{\partial}{\partial r} \left\{\sin \alpha(r) \sin \left[\eta(z - a) + \frac{\pi}{4} - \alpha(r)\right]\right\} dz.$$

In evaluating I_1 and I_2 we will need the relations

$$\int e^{bx} \sin (x + c) \, dx = - \frac{e^{bx}}{b^2 + 1} \left[\cos (x + c) - b \sin (x + c)\right], \tag{18}$$

$$\sin x \sin y = \frac{1}{2} \left[\cos (x - y) - \cos (x + y)\right], \tag{19}$$

and

$$2 \sin\left(x + \frac{\pi}{4}\right) = \sin x + \cos x. \tag{20}$$

By the transformation of variables

$$\bar{z} = \eta(z - a), \qquad d\bar{z} = \eta\, dz, \tag{21}$$

I_1 can be integrated by Eq. (18) to yield a sum of the sine and cosine of the same angle. Using Eq. (20), this can be converted to the sine of the angle plus $\pi/4$. Since the angle already contained $\pi/4$, it now contains $\pi/2$ and can be converted to the cosine. Applying the limits then yields

$$I_1(r, z) = \frac{\sin \alpha(r)}{\eta} \left\{\cos \alpha(r) - e^{-\eta(z-a)} \cos\left[\eta(z - a) - \alpha(r)\right]\right\}. \tag{22}$$

(Remember that in the core η = constant.)

Next apply Eq. (19) to the argument of the r-derivative of I_2. Since η = constant, the term containing the cosine of the sum is independent of r. Thus

$$I_2(r, z) = 2 \frac{\partial \alpha}{\partial r}(r) \int_a^z e^{-\eta(z-a)} \sin\left[\eta(z - a) + \frac{\pi}{4} - 2\alpha(r)\right] dz,$$

and again applying the same procedure yields

$$I_2(r, z) = \frac{1}{\eta} \frac{\partial \alpha}{\partial r}(r) \left\{\cos\left[2\alpha(r)\right] - e^{-\eta(z-a)} \cos\left[\eta(z - a) - 2\alpha(r)\right]\right\}. \tag{23}$$

Free Vortex Region, $r \geq r_c$:

$$V_c = \frac{r_c}{r} V_m \quad \text{and} \quad \omega_c = \frac{V_c}{r} = \frac{V_m r_c}{r^2}.$$

Therefore

$$\eta = \eta(r) = \sqrt{\frac{r_c V_m}{2\nu}}\, \frac{1}{r},$$

and from Eq. (16) the vertical velocity is given by

$$w(r, z) - w(r, a) = V_m \left(\frac{r_c}{r}\right) I_3(r, z), \tag{24}$$

in which

$$I_3(r, z) \equiv 2 \int_a^z \frac{\partial}{\partial r} \left\{\sin \alpha(r) \sin\left[\eta(r)(z - a) + \frac{\pi}{4} - \alpha(r)\right] e^{-\eta(r)(z-a)}\right\} dz.$$

This integration is more difficult since $\eta = \eta(r)$. Applying Eq. (19), noting that $\frac{\partial \eta}{\partial r} = \frac{-\eta}{r}$ yields

$$I_3(r, z) = I_2(r, z) - \frac{1}{\sqrt{2}r} \int_a^z \eta(z - a)\, e^{-\eta(z-a)}\, f(r, z)\, dz$$

where

$$f(r, z) = \left\{ \sin\left[\eta(z - a) + \frac{\pi}{4}\right] + \cos\left[\eta(z - a) + \frac{\pi}{4}\right] - \sin\left[\eta(z - a) + \frac{\pi}{4} - 2\alpha\right] - \cos\left[\eta(z - a) + \frac{\pi}{4} - 2\alpha\right] \right\}.$$

Application of Eq. (20) to f(r, z) yields two terms of the form sin (y + $\pi/2$), which we replace with cosine terms. Then Eq. (19) is used to combine the two cosines to produce a product of sine terms, yielding

$$I_3(r, z) = I_2(r, z) + \frac{2 \sin \alpha}{\eta r} \int_0^{\bar{z}} \bar{z} \sin(\bar{z} - \alpha)\, e^{-\bar{z}}\, d\bar{z},$$

where transformation Eq. (21) has been used in the integral. Defining

$$I_4(r, z) \equiv \int_0^{\bar{z}} \bar{z} \sin(\bar{z} - \alpha)\, e^{-\bar{z}}\, d\bar{z},$$

two integrations by parts of the terms containing $\bar{z}$ yields

$$2I_4 = -\bar{z}\, e^{-\bar{z}} \left[\sin(\bar{z} - \alpha) + \cos(\bar{z} - \alpha)\right]_0^{\bar{z}} + \int_0^{\bar{z}} e^{-\bar{z}} \left[\sin(\bar{z} - \alpha) + \cos(\bar{z} - \alpha)\right] d\bar{z}.$$

Use of Eq. (20) permits evaluation of the remaining integral by Eq. (18).

Evaluation of limits of integration and converting back to z yields

$$I_3(r, z) = I_2(r, z) + \frac{\sin \alpha}{\eta r} \left\{ \cos \alpha - e^{-\eta(z-a)} \left[\sqrt{2}\, \eta(z - a) \sin\left(\eta(z - a) - \alpha + \frac{\pi}{4}\right) + \cos\left(\eta(z - a) - \alpha\right)\right] \right\}. \quad (25)$$

Through Eqs. (17), (22), (23), (24), and (25), the variation of the vertical velocity is now known everywhere in the Ekman inflow layer; but we need yet to determine w(r, a), its value at the lower boundary, the top of the Prandtl layer z = a.

THE PRANDTL LAYER

In the thin Prandtl layer adjacent to the ground the motion is governed by the viscous drag on the lower and upper surfaces of the layer. We use the Prandtl assumptions that the density is constant; that stress, velocity and shear are parallel; and that there exists a mixing length, ℓ, which is a statistical measure of the linear dimensions of the turbulent motions. This yields, for the stress,

$$\tau = \rho \ell^2 \left(\frac{dV}{dz}\right)^2.$$

It is further assumed that the mixing length

$$\ell = k(z + z_0),$$

where $k = 0.4$. Solving for V gives

$$V = \frac{1}{k}\sqrt{\frac{\tau}{\rho}}\log\left(\frac{z + z_0}{z_0}\right)$$

requiring that $V = 0$ at $z = z_0$. The constant z_0 is a measure of surface roughness.* By taking the ratio of the velocity at a level $z < a$ to the velocity at the base of the Ekman layer $z = a$, we obtain

$$\vec{V}(r, z) = V_0\, e^{i\alpha(r)}\, F(z),$$

where

$$F(z) = \left(\frac{\log\dfrac{z + z_0}{z_0}}{\log\dfrac{a + z_0}{z_0}}\right).$$

Combing this with Eq. (9) yields

$$\begin{Bmatrix} u(r, z) \\ v(r, z) \end{Bmatrix} = \begin{Bmatrix} \sin\alpha \\ \cos\alpha \end{Bmatrix} V_c(r)(\cos\alpha - \sin\alpha)\, F(z). \tag{26}$$

The radial inflow in the Prandtl layer is given by Eq. (26), which through a trigonometric simplification becomes

$$u(r, z) = \frac{1}{2} V_c(r)\left[\sqrt{2}\sin\left(2\alpha + \frac{\pi}{4}\right) - 1\right] F(z). \tag{27}$$

Integrating the continuity Eq. (15) from $z = 0$ to $z < a$, and using Eq. (27) and $V_c(r)$ from Fig. 7, we obtain, for the vertical velocity in the Prandtl layer,

*For large-scale motions, $a \approx 10$ m, $z_0 \approx 10$ cm. For the dust devil we expect $a \approx 1$ m, so $z_0 \approx 1$ cm appears reasonable (Byers,[8] p. 605).

$$w(r, z) = -\frac{V_m}{r_c}\left\{1 - \sqrt{2}\left[\sin\left(2\alpha + \frac{\pi}{4}\right) + r\cos\left(2\alpha + \frac{\pi}{4}\right)\frac{\partial\alpha}{\partial r}\right]\right\} G(z) \qquad 0 < r < r_c \qquad (28)$$

$$w(r, z) = \frac{V_m r_c}{r}\sqrt{2}\cos\left(2\alpha + \frac{\pi}{4}\right)\frac{\partial\alpha}{\partial r}\, G(z) \qquad r > r_c$$

where

$$G(z) = \int_0^z F(z)\, dz = \frac{z_0}{\log\left(1 + \frac{a}{z_0}\right)}\left[\left(1 + \frac{z}{z_0}\right)\log\left(1 + \frac{z}{z_0}\right) - \frac{z}{z_0}\right].$$

Discussion of Results

SPECIFICATION OF $\alpha(r)$ AND $\eta(r)$

In order to calculate the velocity fields, the parameters $\alpha(r)$, the inflow angle at the top of the Prandtl layer, and $\eta(r) = \left(\frac{\omega_c(r)}{2\nu}\right)^{1/2}$, the Ekman length based on the cyclostrophic angular velocity $\omega_c(r)$, must be determined from observations. Figure 8 shows an approximate typical distribution for $\alpha(r)$ from discussion in Sinclair[3] (p. 117),

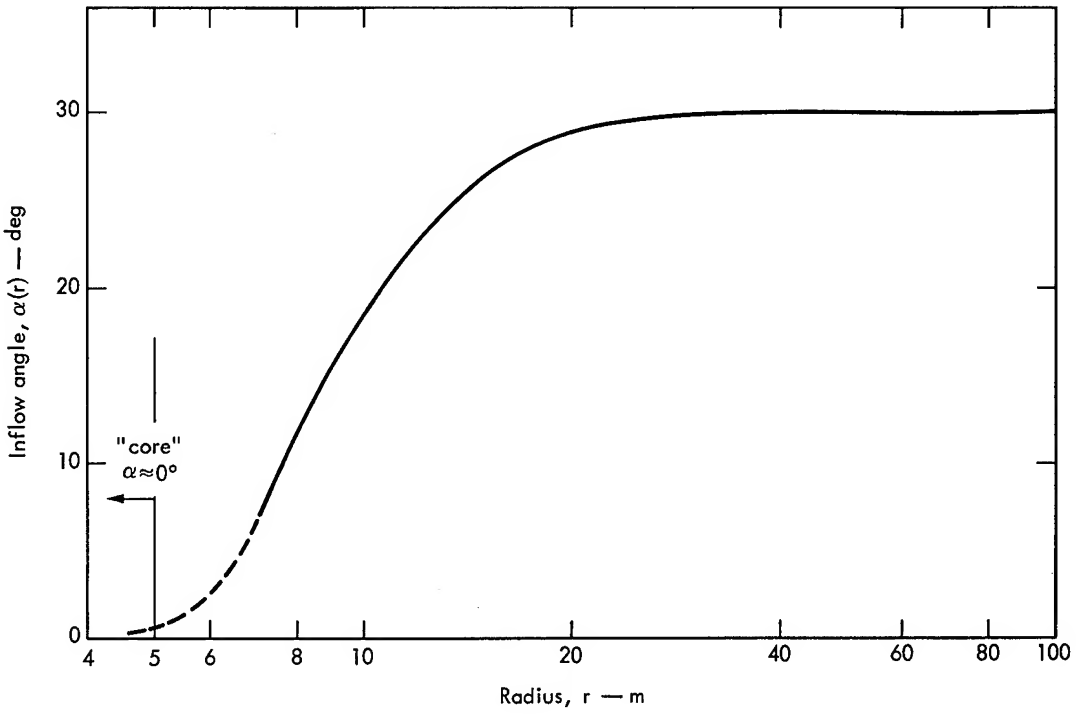

Fig. 8. Approximate distribution of $\alpha(r)$ inflow angle at top of Prandtl layer, from Sinclair's "A quantitative analysis of the dust devil," p. 117).

who indicates that the inflow angle is approximately 30° at large distances ($r > 50$ m) and about 20° for $r \approx 10$ m, and approaches zero within the dust column. Sinclair also comments that at times considerable outflow may occur in the core, which might mean that our Prandtl-layer flow angle α had changed sign. Such an outflow would force the often-observed downdraft in the core by continuity. However, Sinclair points out that there is no systematic radial outflow, and the observations presented in Fig. 2 indicate oscillations in the sign of u in the core. Because of this uncertainty in the exact value for α in the core we use an average value of $\alpha \approx 0$ in the core and will not attempt to obtain any downdraft in our results. Also, and perhaps more importantly, the approach used in this paper, while quite good for describing the basic velocity fields in the dust devil, is probably not capable of properly analyzing the core downdraft phenomenon. If, as Sinclair[3] speculates (p. 112), this downdraft is a region of somewhat cooler air embedded in the warm central region of the dust devil, a correct description of this must also include the energy equation, which has not been required in the present analysis.

Specification of $V_c(r)$, the velocity distribution in the cyclostrophic region above the Ekman and Prandtl boundary layers, determines $\omega_c(r)$ and thus $\eta(r)$. For the following calculations, $V_c(r)$ is taken from the distribution shown in Fig. 3b, which is very nearly the velocity distribution in the cyclostrophic region.

(Although in the present analysis $\alpha(r)$ and $\eta(r)$ are specified independently, it is interesting to note that they can be related using Eq. (9) which contains μ, $\eta(r)$, $\alpha(r)$, and κ, a proportionality constant from Prandtl's assumption, Eq. (6). Assuming κ is known, Eq. (9) may be rewritten to yield $\alpha(r)$ in terms of $\eta(r)$, i.e.,

$$\cot \alpha(r) = 1 + 2\kappa\mu\eta(r).$$

One might choose $\kappa = 0.2$ cm^2/sec/g^{-1}, which gives $\alpha \approx 20°$ for $\mu = 200$ g/cm^{-1}/sec^{-1} and $\eta = 0.02$ cm^{-1}. However, for the present work it is preferrable to leave $\alpha(r)$ a parameter to be specified from experimental observations.)

HEIGHT OF THE EKMAN LAYER AND BASIC BOUNDARY LAYER BEHAVIOR OF u, v, AND w

Using the above values for $\alpha(r)$ and $\eta(r)$, the top of the Ekman inflow layer, $H(r)$, is calculated from Eq. (12), and plotted in Fig. 9, which shows nearly constant (approximately 12 m) thickness in the core and rapid growth outside.

Typical radial and tangential velocities in the Ekman and Prandtl layers are computed from Eqs. (11) and (26) and plotted in dimensionless form in Fig. 10. The radial velocity profile is most interesting, taking its maximum value near the ground and rapidly decaying as the top of the Ekman layer is approached. The variation of vertical velocity with height near the edge of the dust devil core is shown in Fig. 11.

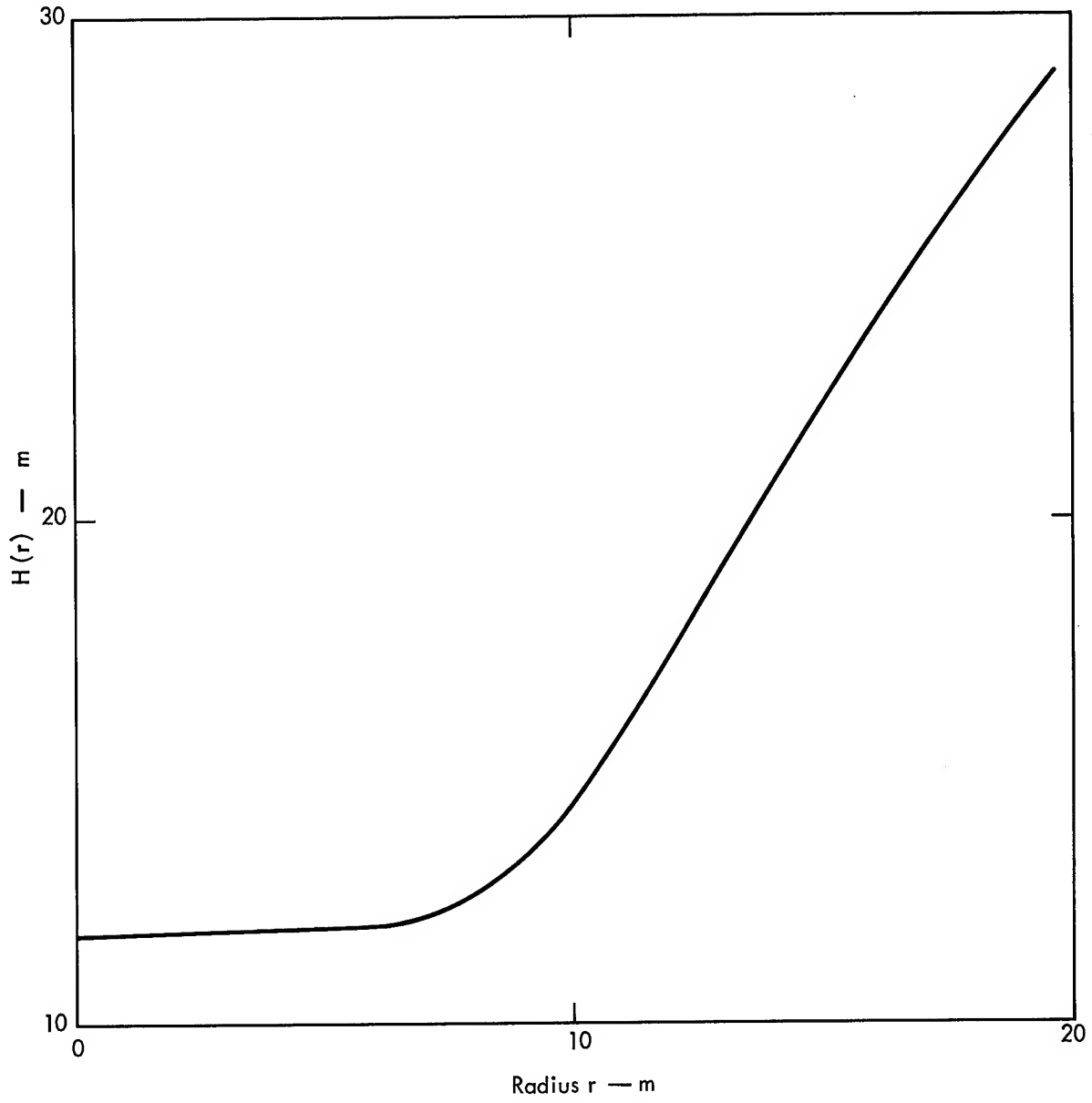

Fig. 9. Top of Ekman inflow layer H(r) vs radius r for dust devil data from Figs. 4 and 8 (V_m = 13 m/sec, r_c = 9 m, a = 1 m, ν = 15 m^2/sec).

COMPARISON WITH KUO

Kuo[5] has developed a simplified system of equations for atmospheric convection problems by expanding the flow variables in powers of two small parameters defined by the percentual variances of the equivalent potential temperature and density. He then investigated convective atmospheric vortices by introducing a thick layer of unstable stratification and a large vorticity as the basic elements for the creation and maintenance

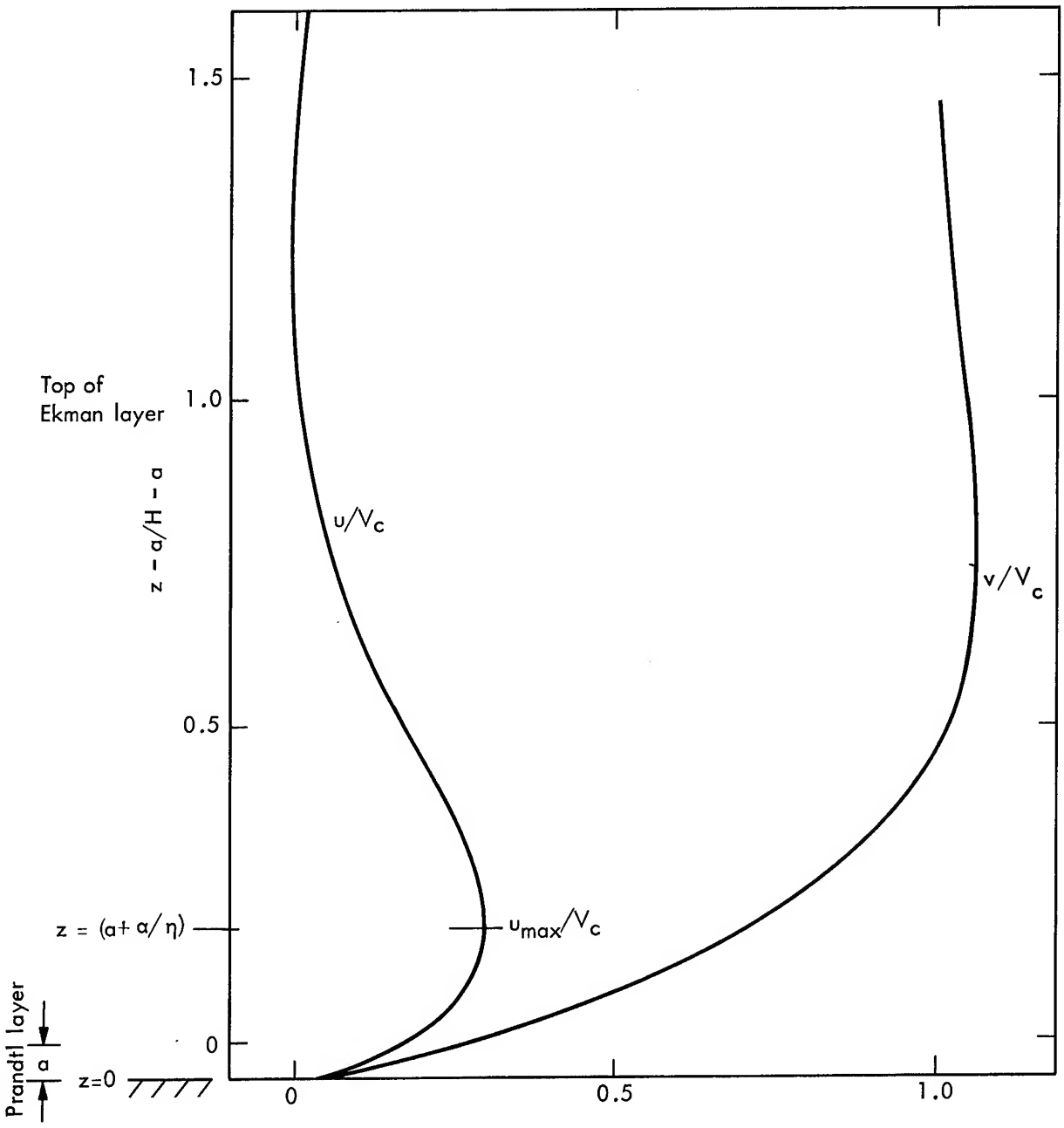

Fig. 10. Typical radial (u) and tangential (v) velocity profiles in the Ekman and Prandtl layers. (Computed for r = 13.3 m, V_c = 10 m/sec, α = 30°, ν = 15 m^2/sec, a = 1 m.)

of such vortices. Although primarily interested in tornadoes which have such a thick unstable layer, he claimed that, to the accuracy considered, his model should also describe lesser storms such as dust devils and whirlwinds resulting from unstable stratification in a much thinner layer. In spite of his more sophisticated approach and different emphasis, his first-order boundary-layer analysis yields similar profiles for

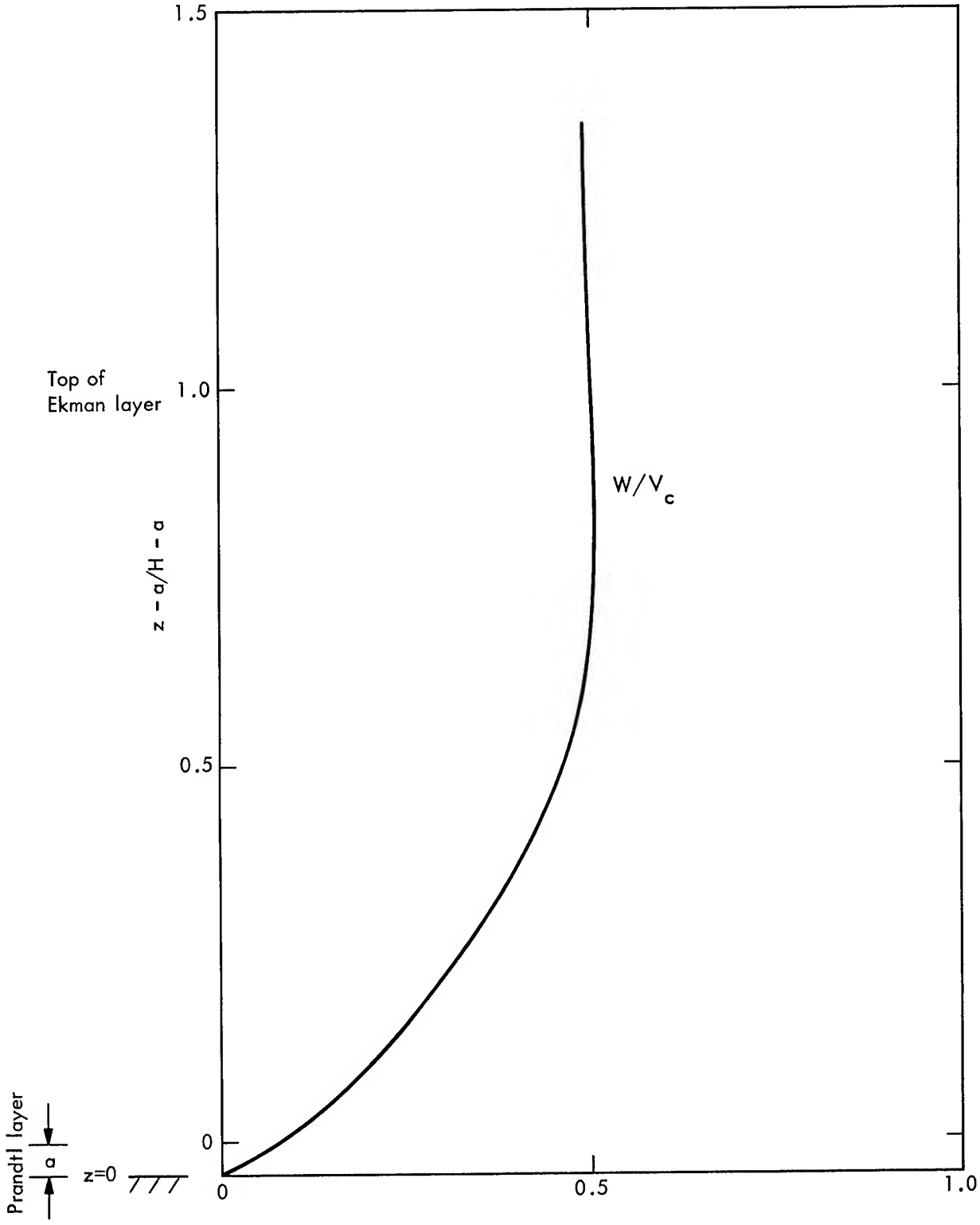

Fig. 11. Variation of vertical velocity with height near the edge of dust devil core, $r \approx r_c$. (Computed for $r = 6$, $V_c = 13$, $\alpha = 0°$, $\partial\alpha/\partial r = 6°/m$, $\nu = 15\ m^2/sec$, $a = 1$ m.)

the velocity components and qualitatively the same behavior for the boundary-layer thickness, reproduced in Fig. 12 (compare to Figs. 9, 10, and 11).

This agreement lends support to the solution obtained in the present model and should indicate that most probably Kuo's solution does hold for dust devils, provided the scale is properly reduced by inclusion of a thin, highly unstable thermal layer and less inherent vorticity than that found in the tornado.

DETAILED VELOCITY COMPONENT BEHAVIOR AND COMPARISON TO SINCLAIR'S MEASUREMENTS

Figure 13 shows the computed radial variation of the tangential, radial, and vertical velocity components near the bottom of the Ekman inflow layer. The maximum tangential velocity is seen to be approximately 10% less than the maximum tangential velocity in the cyclostrophic region. This again justifies the linearizing assumption

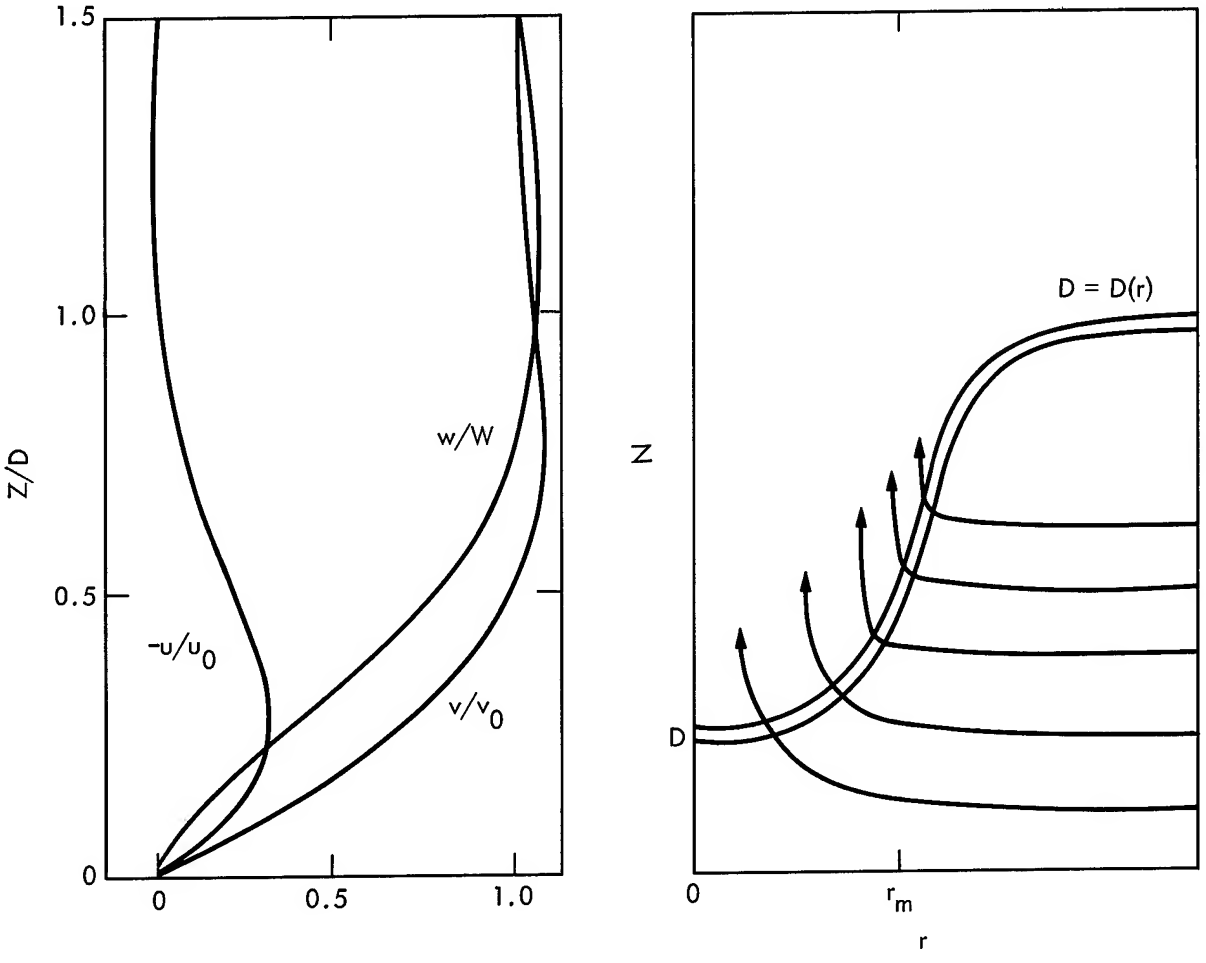

(a) Velocity components u, v, w.

(b) Boundary layer thickness.

Fig. 12. Kuo's boundary layer results (from "On the dynamics of convective atmospheric vortices").

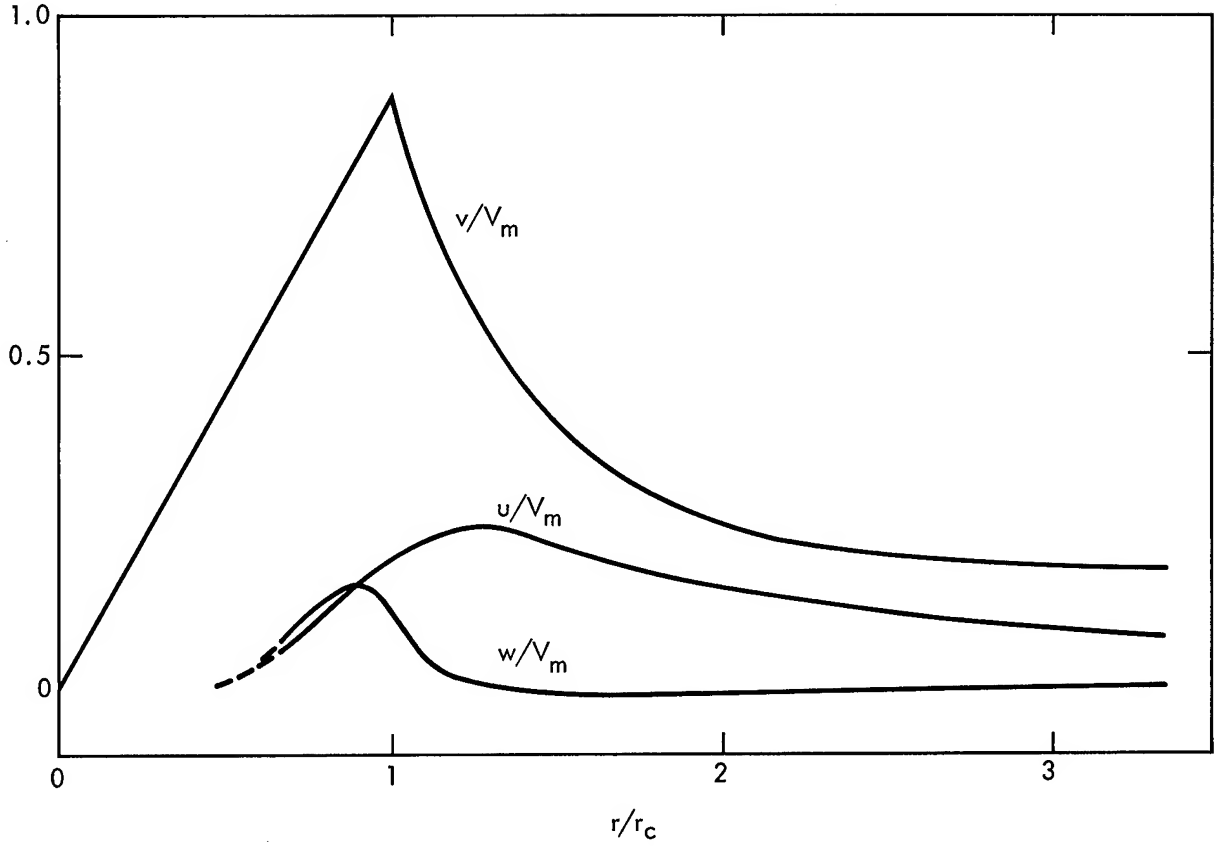

Fig. 13. Behavior of the tangential, radial, and vertical velocity components near the bottom of the Ekman inflow layer, $z/r_c = 0.222$. Dashed lines indicate probable behavior, not calculated due to uncertainty in $\alpha(r)$. (Computed for $V_m = 13$ m/sec, $r_c = 9$ m, a = 1 m, $\nu = 15$ ft^2/sec.)

that ω is constant in the boundary layer, initially made on the basis of experimental observations.*

Figure 13 demonstrates the experimentally verified facts (Sinclair,[3] p. 117) that the radial velocity reaches its maximum outside of v_{max} and w_{max}, and whereas w decays very rapidly from its maximum value, u decays very much slower. Also according to the figure, the region of w_{max} occurs within v_{max}, as Sinclair[3] shows actually occurs (p. 114).

From Fig. 13 we deduce that in the boundary layer the environmental air spirals toward the low-pressure center with essentially horizontal motion (even with perhaps slight downward velocity) until it reaches the vicinity of the dust column, where it enters the region of w_{max} and thus begins rising rapidly in a helical motion of almost constant radius. Sinclair[3] states (p. 117) that this is indeed what happens.

The magnitude of u appears consistent with experimental values about 3-4 m/sec if V_m is 13-15 m/sec. However, the corresponding maximum value for w, 2 m/sec,

*However, Sinclair's measurements, Fig. 3, show a slight increase in maximum amplitude of v at the lower level, contrary to what one would expect from the boundary-layer analysis, cf. Fig. 10. This minor discrepancy is not deemed serious and will not be pursued further.

is smaller than experiments indicate can occur at this level (5-10 m/sec from Fig. 2). Possible reasons the theoretical w is too small are the approximate (and not quite correct) distribution for $\alpha(r)$ near the core and the assumption of axial symmetry, perhaps not too good if the dust devil is sloped and moving.

However, a calculation of w above the boundary layer where the radial velocity is negligible, given in Fig. 14, shows a marked increase in magnitude (to nearly 8 m/sec for V_m = 13 m/sec), which is much closer to experimentally observed values.

It is also interesting to note that lower in the boundary layer the v profile is steeper or more cuspy near v_{max} (at r_c) than it is higher, as seen by comparing v in Figs. 13 and 14. Sinclair's experimental measurements in Fig. 3 also indicate this behavior.

A physical visualization of the radial variation of the inflow u is given in Fig. 15, where computed nondimensional u profiles are shown at their respective nondimensional distances from the vortex axis r = 0. Also shown are the line of $u_{max}(r)$ from Eq. (13), the top of the Ekman layer H, and a typical-sized dust column (from Sinclair,[3] Fig. 2). Interestingly, according to Sinclair's[3] measurements, Fig. 2, the edge of the dust column, r_d, occurs within the radius of maximum tengential velocity, r_c. (From Figs. 2 and 3: at z = 7 ft, r_d = 2.6 m, r_c = 5 m; at z = 31 ft, r_d = 5.3 m, r_c = 9 m.)

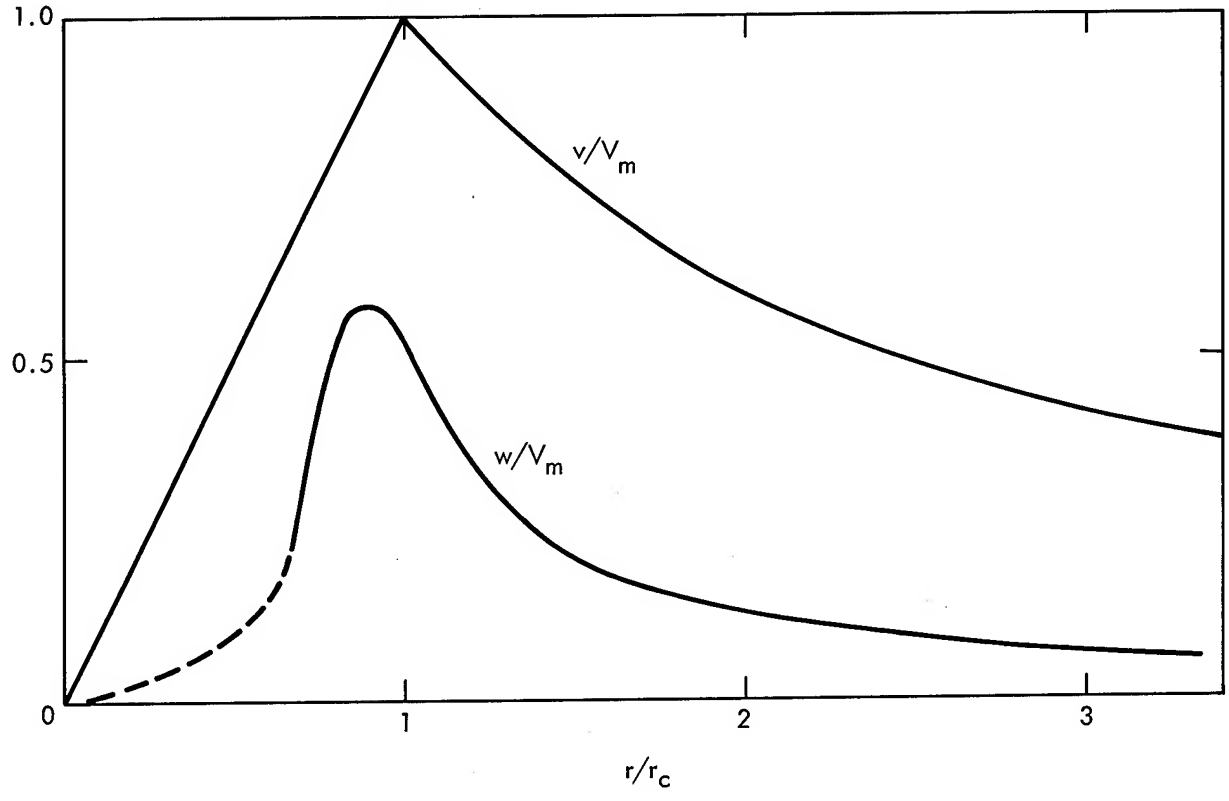

Fig. 14. The tangential and vertical velocity components above the Ekman layer in the cyclostrophic region. The radial velocity is negligible and the superposition of the v and w velocity fields would result in a helical motion. Dashed lines indicate probable but uncalculated behavior. (Computed for V_m = 13 m/sec, r_c = 9 m, a = 1 m, ν = m^2/sec.)

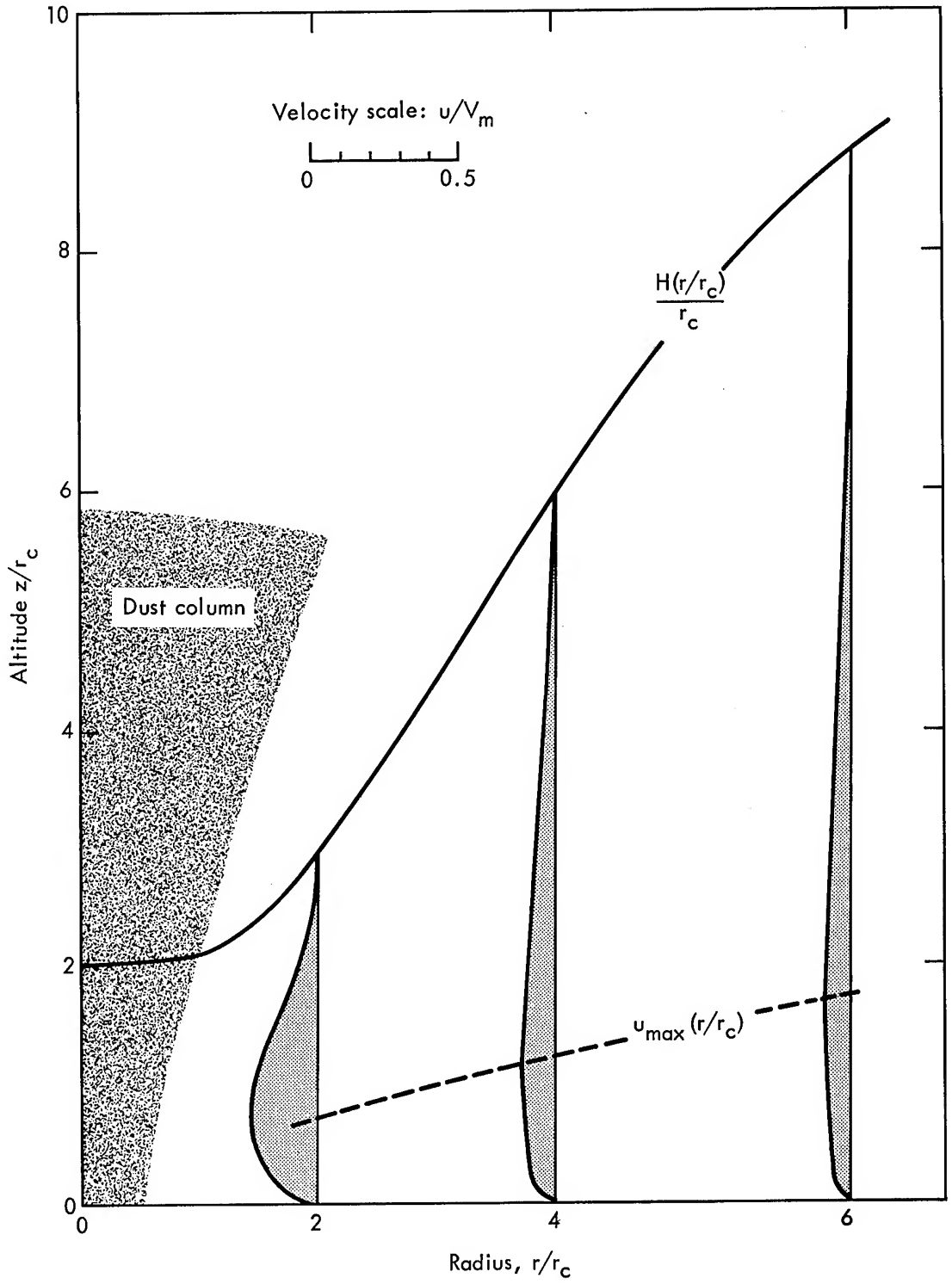

Fig. 15. Variation of inflow profiles with radius, showing line of maximum u, top of Ekman layer H, and dust column (from Sinclair's "A quantitative analysis of the dust devil," Fig. 2). The velocity is nondimensionalized with respect to V_m and lengths with respect to r_c. (Computed for V_m = 13 m/sec, r_c = 6 m, a = 1 m, ν = 15 m^2/sec, V_c from Fig. 3b.)

Sinclair states that he observed radial inflow at all levels (z = 7, 17, 31 ft) except on the "forward" (with respect to direction of motion of the dust devil) side of the 31-ft level, where radial outflow was observed. He observes that this was due to the sloping of the dust devil resulting from wind shear.* Perhaps also part of the "inflow" observed behind the dust devil at this height could be a wake effect resulting from wake momentum deficiency (as in Schlicting,[9] Ch. XXIII). From our boundary-layer analysis, which implicitly assumes a vertical, stationary† dust devil, we would expect only a small inflow at z = 31 ft (or approx. 10 m), not more than 1 to 1-1/2 m/sec, from Fig. 15.

A diagram for the vertical-velocity variation with height is shown in Fig. 16, illustrating the radial expansion with altitude of the region of upward vertical motion that Sinclair[3] (pp. 113-114) states appears similar to the radial expansion of a turbulent jet by entrainment. In our model, the radius at which w_{max} occurs remains constant, since we have assumed r_c to be constant throughout the boundary layer. A more complicated model might attempt to obtain this funnel shape by setting $r_c = r_c(z)$, but this would be empirical and thus quite unsatisfying.

Conclusions

It has been shown that the cyclostrophic-wind equation, Eq. (2), can be linearized for the dust devil to produce a simple analytical result for the velocity fields, which agrees with a boundary-layer result of Kuo and yields good qualitative and semi-quantitative agreement with the observations and measurements of Sinclair. The linearization was justified first by experimental measurements and then later by the solution itself. The analytical result depends functionally on two parameters $\alpha(r)$ and $\eta(r)$, obtainable from experimental data.

An obvious and practical extension of this model would be to develop a perturbation-expansion solution in a more systematic manner; so the present result appeared as the first-order solution, and a correction term was obtainable by consideration of second-order terms. Also, since our model cannot properly describe the core downdraft and does not deal explicitly with the thin, unstable, thermal boundary layer, a more sophisticated analysis should include an energy equation and equation of state, which might then yield temperature and density fields. Apparently Kuo[5] has made such an attempt with some success.

---

*According to Sinclair[3] (p. 121), sloping dust devils are more frequent than vertical ones.

† More accurately, we have assumed a coordinate system fixed to and moving with the dust devil.

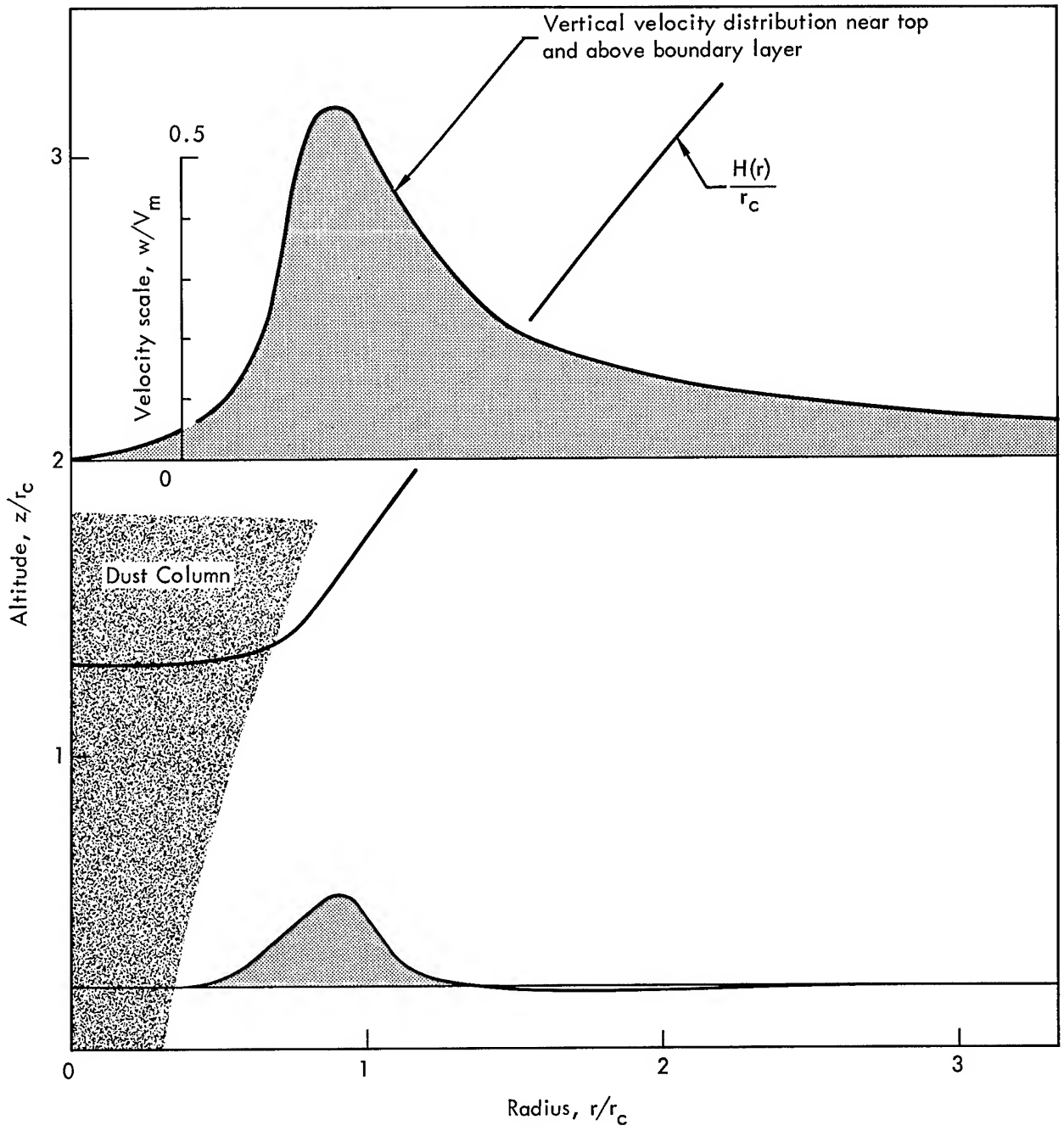

Fig. 16. Vertical velocity distributions near bottom and top of the Ekman layer shown in relation to the dust column and H. Velocity is nondimensionalized with respect to V_m and length with respect to r_c. Velocity profiles are taken from Figs. 13 and 14. (Computed for V_m = 13 m/sec, r_c = 9 m, a = 1 m, ν = 15 m^2/sec, $V_c(r)$ from Fig. 3b.)

Acknowledgments

My sincere thanks to Hugh W. Ellsaesser, whose suggestion of the problem, patience, and careful checking made the work possible. Also my thanks to Mildred Rundquist, who bravely read my script and cheerfully typed it twice.

References

1. I. Michelson, On Dust Devils, Ph. D. Thesis, California Institute of Technology (1951).
2. R. L. Ives, "Behavior of the Dust Devil," Bull. Am. Meteorol. Soc. 28, 168-174 (1947).
3. P. C. Sinclair, A Quantitative Analysis of the Dust Devil, Ph. D. Thesis, University of Arizona (1966).
4. P. C. Sinclair, "General Characteristics of Dust Devils," J. Appl. Meteorol. 8, 32-45 (1969).
5. H. L. Kuo, "On the Dynamics of Convective Atmospheric Vortices," J. Atmospheric Sci. 23, 25-42 (1969).
6. H. W. Ellsaesser, "An Approach to the Study of the Energy Cycle in a Tropical Cyclone" (Unpublished), University of California (Los Angeles) (1947).
7. G. I. Taylor, (Title not available), Phil. Trans. Roy. Soc. London, Ser. A: 215, 1 (1915).
8. H. R. Byers, General Meteorology (McGraw-Hill, New York, 1944).
9. H. Schlichting, Boundary Layer Theory (Pergaman Press, New York, 1955).
10. P. C. Sinclair, "Some Preliminary Dust Devil Measurements," Monthly Weather Rev. 92, 363-367 (1964).

Distribution

LRL Internal Distribution

Michael M. May	
E. Teller	
W. Hudson	2
W. P. Crowley	
H. W. Ellsaesser	10
J. W. Hardy	
J. Killeen	2
M. C. MacCracken	
M. Newman	
W. H. Plows	
R. J. Stinner	
J. J. Walton	
B. M. Johnston	
W. D. Schulz	
M. Rundquist	2
R, K. Wakerling, Berkeley	
D. Wilkes, Berkeley	
TID Berkeley	
TID File	30

External Distribution

S. E. Logan 10
California Institute of Technology
Pasadena, California

Hsiao-Lan Kuo
University of Chicago
Chicago, Illinois

P. C. Sinclair
Colorado State University
Ft. Collins, Colorado

S. L. Rosenthal
National Hurricane Research Laboratory
Miami, Florida

J. G. Charney
Massachusettes Institute of Technology
Cambridge, Massachusettes

A. Barcilon
General Electric Company
King of Prussia, Pennsylvania

External Distribution (Continued)

H. Lettan
University of Wisconsin
Madison, Wisconsin

K. Oayama
New York University
New York, New York

TID-4500 Distribution, UC-53, Meteorology

163

Printed in USA. Available from the Clearinghouse for Federal Scientific and Technical Information, National Bureau of Standards, U. S. Department of Commerce, Springfield, Virginia 22151
Price: Printed Copy $3.00; Microfiche $0.65.

LF/rd